Carbon Footprint Enhancement of an Agricultural Telehandler through the Application of a Fuel Cell Powertrain

World Electric Vehicle Journal

MDPI

Article

Carbon Footprint Enhancement of an Agricultural Telehandler through the Application of a Fuel Cell Powertrain

Valerio Martini †, Francesco Mocera *,† and Aurelio Somà †

Departiment of Mechanical and Aerospace Engineering (DIMEAS), Politecnico di Torino, Corso Duca degli Abruzzi 24, 10129 Torino, Italy; valerio.martini@polito.it (V.M.); aurelio.soma@polito.it (A.S.)

* Correspondence: francesco.mocera@polito.it

† These authors contributed equally to this work.

Abstract: The growing awareness about climate change and environmental pollution is pushing the industrial and academic world to investigate more sustainable solutions to reduce the impact of anthropic activities. As a consequence, a process of electrification is involving all kind of vehicles with a view to gradually substitute traditional powertrains that emit several pollutants in the exhaust due to the combustion process. In this context, fuel cell powertrains are a more promising strategy, with respect to battery electric alternatives where productivity and endurance are crucial. It is important to replace internal combustion engines in those vehicles, such as the those in the sector of Non-Road Mobile Machinery. In the present paper, a preliminary analysis of a fuel cell powertrain for a telehandler is proposed. The analysis focused on performance, fuel economy, durability, applicability and environmental impact of the vehicle. Numerical models were built in MATLAB/Simulink and a simple power follower strategy was developed with the aim of reducing components degradation and to guarantee a charge sustaining operation. Simulations were carried out regarding both peak power conditions and a typical real work scenario. The simulations' results showed that the fuel cell powertrain was able to achieve almost the same performances without excessive stress on its components. Indeed, a degradation analysis was conducted, showing that the fuel cell system can achieve satisfactory durability. Moreover, a Well-to-Wheel approach was adopted to evaluate the benefits, in terms of greenhouse gases, of adopting the fuel cell system. The results of the analysis demonstrated that, even if considering grey hydrogen to feed the fuel cell system, the proposed powertrain can reduce the equivalent CO_2 emissions of 69%. This reduction can be further enhanced using hydrogen from cleaner production processes. The proposed preliminary analysis demonstrated that fuel cell powertrains can be a feasible solution to substitute traditional systems on off-road vehicles, even if a higher investment cost might be required.

Keywords: fuel cell; hydrogen; GHG emissions reduction; hybrid electric vehicle; telehandler; innovative powertrain; Non-Road Mobile Machineries

Citation: Martini, V.; Mocera, F.; Somà, A. Carbon Footprint Enhancement of an Agricultural Telehandler through the Application of a Fuel Cell Powertrain. *World Electr. Veh. J.* **2024**, *15*, 91. https://doi.org/10.3390/wevj15030091

Academic Editors: Fachao Jiang, Yongyu Li and Weiwei Kong

Received: 1 February 2024
Revised: 27 February 2024
Accepted: 28 February 2024
Published: 1 March 2024

1. Introduction

In recent years, the scientific community has deeply investigated the effects of anthropic activities in terms of environmental pollution, as well as the consequences on human health, climate change and economics [1–6]. Indeed, almost all human acitivities involve systems that are sources of emissions. The emissions produced can differ in quantity, depending on the specific pollutant or greenhouse gas under consideration, for the different sectors of anthropic activity. Industry, agriculture and transport sectors are characterized by high emission levels due to the adoption of internal combustion engines, which are required to accomplish several tasks. Indeed, internal combustion engines (ICEs) are one of the major contributors to air pollution, mainly due to fuel extraction processes and by-products of combustion [7,8]. In this context, several efforts are made, both from academic and industrial worlds, to study and develop innovative powertrains with lower

emission levels, in order to reduce the impact related to the transport sector [9]. These efforts are supported by policies that will force the introduction of electric and alternatives powertrains as substitutions for their traditional diesel and gasoline counterparts [10]. If this trend already has a clearly visible effect on passenger cars, with several countries experiencing a quick introduction of electric vehicles on the market [11], the sector of Non-Road Mobile Machinery (NRMM) will still be at an earlier stage of electrification, even if studies have demonstrated that these vehicles have a high impact in terms of life cycle emissions [12,13]. The reason for that is related to the operative requirements that these vehicles must fulfill, with high productivity and endurance that represent a barrier to the development of pure battery electric powertrains [14]. As a consequences, several studies focused on hybrid powertrains [15–19]. Indeed, the hybridization of the powertrain allows for a downsizing of the thermal unit, which can lead to a higher efficiency and better fuel economy. Moreover, the adoption of a smaller engine can allow for simplier aftertreatment systems since the emission limits are usually defined according to the rated power of the ICE. As a consequence, different manufacturers have presented prototypes of hybrid off-road vehicles [20,21]. However, hybrid powertrains featuring the presence of an internal combustion engine still produce several harmful pollutants in the exhaust. To overcome this limit, an alternative solution for the electrification of the sector of NRMM is represented by fuel cell powertrains [22–28]. Fuel cell hybrid electric powertrains have gained attention due to their characteristics that combine the advantage of having approximately zero local emissions with high endurance and low refuelling time [29]. These properties, along with the high energy density of hydrogen, are of particular interest for the sector of NRMM. As a consequence, fuel cells, powered using hydrogen or other fuels, such as ammonia, are a promising solution to decarbonize the so-called hard-to-abate sectors, such as the marimite one [30]. Indeed, fuel cell powertrains can operate for several hours straight, which is a severe operational requirement for off-road vehicles, without having the issue of range anxiety. Moreover, fuel cell systems have higher efficiency with respect to thermal engines; thus, a better fuel economy is expected. From an economical point of view, using hydrogen as fuel can allow for energy independence and self-sufficiency, along with the possibility of defining circular economy scenarios [31]. The most promising type of fuel cell for vehicular applications is the proton-exchange membrane fuel cell (PEMFC), due to its high efficiency, low working temperature, compactness and long operational life [32,33]. However, the benefits of introducing fuel cell systems in terms of greenhouse gases emission reduction strongly depends on the hydrogen production method [34–36], with production through steam methane reforming that, at present, is the most adopted one and contributes to more than 60% of the global hydrogen production [37]. Other issues related to fuel cell systems are represented by their high purchasing costs and the inadequate state of the hydrogen refuelling network, which are two of the major challenges that must be addressed in the near future to promote their diffusion [38,39]. From an applicative point of view, fuel cell powertrains can have different topologies. Indeed, to avoid the fast degradation of fuel cells, one or more auxiliary units, generally batteries or supercapacitors, should be introduced to the powertrain to help manage sudden changes in the external load [40]. Indeed, fuel cell degradation is related to start and stop cycles, idling, high power conditions and load changes [41]. With the introduction of other power sources comes the mandatory development of an energy management strategy (EMS) that must determine how the electrical power requested by the electric motor is split among the different units [42]. Given these premises, in the present paper a fuel cell hybrid electric powertrain for a off-road heavy duty vehicle, namely a telehandler, is presented. The specifications of the traditional vehicle under investigation are defined according to existing and commercially available models. In detail, the Merlo Turbofarmer 42.7 vehicle was taken as a reference for the analysis [43]. This vehicle was designed specifically for agricultural applications. These vehicles are characterized by the presence of an hydraulic system for the actuation of the mechanical arm, thus the total load is determined by the sum of the power requested by the driveline and the power requested by the hydraulic system [44]. The powertrain

architecture is composed of a PEMFC and a battery pack, with DC-DC power converters for the connection of both the fuel cell and the battery pack with the DC bus. As for the EMS, a simple power follower strategy was developed. Numerical models of both the fuel cell powertrain and the traditional counterpart were built in MATLAB/Simulink. Simulations were carried out to evaluate performances and fuel consumptions, in order to compare the two powertrains. Moreover, the environmental impacts, considering the global warming potential, of the two powertrains were compared using Well-to-Wheel (WtW) coefficients for both Diesel and Hydrogen. This paper is structured as follows: Section 2 introduces the case study and the proposed fuel cell powertrain, Section 3 presents the numerical models used for the simulations, Section 4 describes the EMS and the simulated work scenario, Section 5 shows and discusses the results obtained from the simulations, and finally Section 6 summarizes the conclusions.

2. Case Study

2.1. Traditional Vehicle

The traditional vehicle under investigation is a 105 kW diesel-powered telehandler, with a unladen mass of 7800 kg, a maximum load capacity of 4200 kg and a maximum lifting height of 7 m [43]. A telehandler is a machine with a telescopic boom that can be extended to lift, handle and place loads. The boom can be equipped with different implements to complete different tasks depending on the specific application. Due to their properties, telehandlers are widely adopted in the industry sector and in agriculture. Indeed, their particular design configuration allows for moving loads from and to places that are unreachable for the other vehicles. A schematic representation of the powertrain is reported in Figure 1, while the main properties of the vehicle are reported in Table 1. The transmission is a hydrostatic transmission with a variable displacement pump and fixed displacement motor. This type of transmission is adopted since it allows for a continously variable transmission, thus reducing the complexity of the whole driveline, and, moreover, it features high power transmission capabilities without requiring expensive and bulky components. However, the higher power losses with respect to a pure mechanical driveline have a non-neglibile impact on the overall vehicle efficiency. Downstream from the hydrostatic transmission, there is a two-speed gearbox, which allows for operating in low-speed and high-speed conditions. This gearbox is useful for having optimized gear ratios for the two most common work conditions. Indeed, during work scenarios involving the use of the telescopic boom, the vehicle generally operates in a speed range below 15 km/h, while during road transportation it operates at speeds up to 40 km/h. The low-speed regime is also useful for overcoming slopes. As for the hydraulic system for work operations, it comprises a lifting arm and an extension boom.

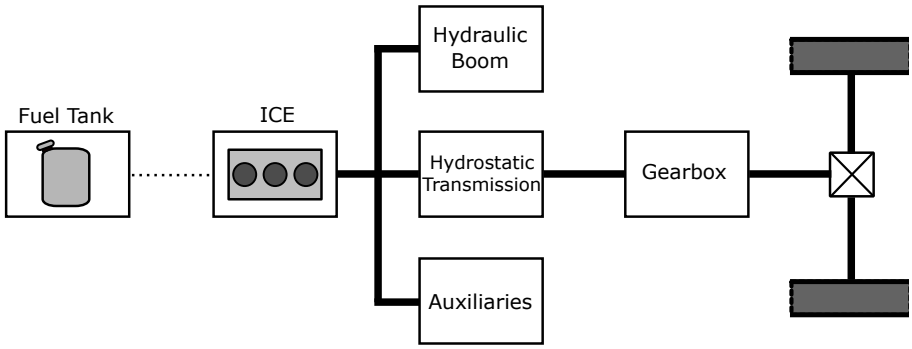

Figure 1. Schematic representation of the traditional reference powertrain.

Table 1. Traditional telehandler's main properties.

Parameter	Value
Unladen Mass	7800 kg
Max Load capacity	4200 kg
Max lift height	7 m
Max vehicle speed	40 km/h
Transmission	Hydrostatic transmission
Diesel Engine	4-cyl 3.6 L 105 kW

2.2. Fuel Cell Hybrid Electric Vehicle

The proposed fuel cell configuration is shown in Figure 2. Apart from the powertrain system, comprising the fuel cell system, the batteries, the power converters and the electric motor, the other elements of the vehicle, namely the hydrostatic transmission, hydraulic system and gearbox, were considered the same as the traditional vehicle. The main properties of the electric motor, fuel cell stack and battery pack for the proposed configuration are reported in Table 2. The fuel cell system was dimensioned considering the average expected power required by the vehicle, to guarantee a high productivity comparable with that of the traditional counterpart. As for the battery pack, it was sized to have enough power capabilities to satisfy sudden and abrupt changes in the power request without excessive C-rates. Indeed, considering a discharge current of 5C, the battery pack is able to provide an electric power that is equal to 75% of the electric motor nominal power. Moreover, the two units were selected considering reasonable space availability constraints for the on-board integration. The vehicle mass was assumed to be the same, or at least not substantially different, as the traditional case.

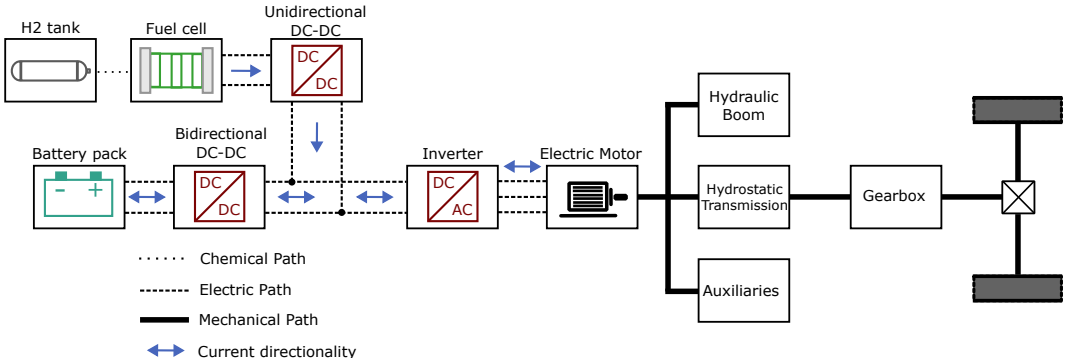

Figure 2. Schematic representation of the fuel cell hybrid electric powertrain.

Table 2. Proposed fuel cell powertrain main properties.

Element	Parameter	Value
Fuel cell system	Stack max power	53 kW
	Number of cells	300
	Max operating point	312.5 A @ 170 V
	Stack efficiency	47.5% @ 50 kW
Battery Pack	Rated Capacity	50 Ah
	Rated Voltage	320 V
Electric Motor	Rated Power	105 kW
	Rated Torque	502 Nm
	Maximum Efficiency	95%

3. Numerical Modelling

3.1. Traditional Vehicle Numerical Modelling

The numerical models were built in MATLAB/Simulink using the Simscape tool. As a consequence, a Physical Network modelling approach was used [45]; thus, each entity is considered as a physical entity capable of exchanging energy with all the other elements to which it is connected. The same modelling approach was used for previous studies from the author's research group [15,16,18,22]. During the development of the numerical model, the following aspects were covered:

- Vehicle dynamics;
- Transmission;
- Hydro-mechanical system;
- Lifting arm and extension boom;
- Engine power output and fuel consumption.

As for the vehicle dynamics, the approach adopted by the authors consisted of a 1D longitudinal model, represented in Figure 3, and was characterized by the following equations:

$$m\dot{V}_x = 2(F_{xf} + F_{xr}) - F_{aero} - mg \cdot sin(\beta) \tag{1}$$

$$F_{zf} = \frac{-h(F_{aero} + mg \cdot sin\beta) + b \cdot mg \cdot cos(\beta)}{2(a+b)} \tag{2}$$

$$F_{zr} = \frac{+h(F_{aero} + mg \cdot sin\beta) + a \cdot mg \cdot cos(\beta)}{2(a+b)} \tag{3}$$

where:

- a, b, and h represent the relative position of the center of gravity of the vehicle with respect to the front and rear axles.
- m is the tractor mass; g is the acceleration of gravity.
- β is the road slope angle.
- V_x is the vehicle longitudinal speed.
- F_{aero} is the aerodynamic drag force as $F_{aero} = 0.5\rho C_d A {V_x}^2 sign(V_x)$, with ρ being the air density, C_d being the drag coefficient and A being the frontal cross-sectional area of the vehicle.
- F_{xf} and F_{xr} are the contact forces between the wheels and the ground on the longitudinal direction (front and rear axel); these forces are determined by the tire–soil interaction.
- F_{zf} and F_{zr} are the contact forces between the wheels and the ground on the longitudinal direction (front and rear axel).

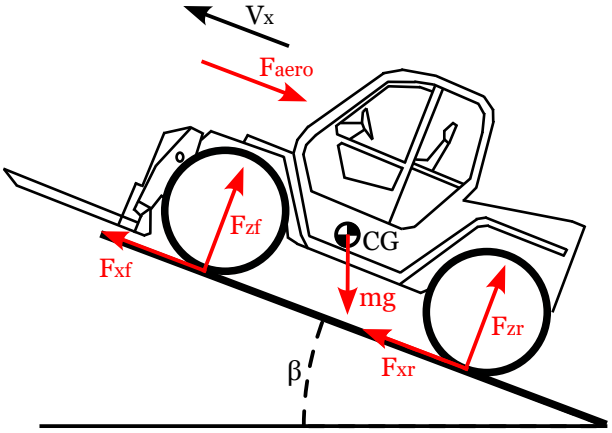

Figure 3. One-dimensional longitudinal model for the vehicle dynamics.

The contact between the tires and the soil was parameterized in terms of static and kinetic coefficients. The first determines the applied torque at which the tire loses traction and begins to slip, and the second determines the amount of torque the tire transmits to the pavement once it begins to slip. Thus, the traction force was evaluated according to the following equations:

$$F_{xi} = \begin{cases} \frac{T_{wheel}}{R_{wheel}} & \text{if } \frac{T_{wheel}}{R_{wheel}} \leq \mu_{static} * F_{zi} \\ \mu_{kinetic} * F_{zi} & \text{if } \frac{T_{wheel}}{R_{wheel}} > \mu_{static} * F_{zi} \end{cases} \quad (4)$$

where F_{xi} is the traction force on the i-axle, F_{zi} is the normal force on the i-axle, T_{wheel} is the torque at the wheel downstream from the driveline, R_{wheel} is the wheel radius, and μ_{static} and $\mu_{dynamic}$ are, respectively, the static and kinetic friction coefficients.

As for the transmission, the hydrostatic transmission was modelled considering three main elements: a variable displacement pump, a fixed displacement motor and a pressure relief valve. The characteristics considered for those elements are reported in Table 3. The no-load torque and friction torque vs. pressure gain/drop coefficients of the hydraulic units were modelled so that the hydrostatic transmission was characterized by the efficiency curve shown in Figure 4. That efficiency curve was obtained considering that the datasheets of hydraulic pumps and motors had similar applications and nominal specifications in the proposed case study.

Table 3. Hydrostatic transmission characteristics.

Parameter	Value
Pump max displacement	150 cm^3
Motor displacement	150 cm^3
Pump nominal pressure gain	250 bar
Motor nominal pressure drop	250 bar
Pump and motor nominal shaft speed	2000 rpm
Pump nominal volumetric efficiency	92%
Motor nominal volumetric efficiency	92%
Valve pressure setting	300 bar

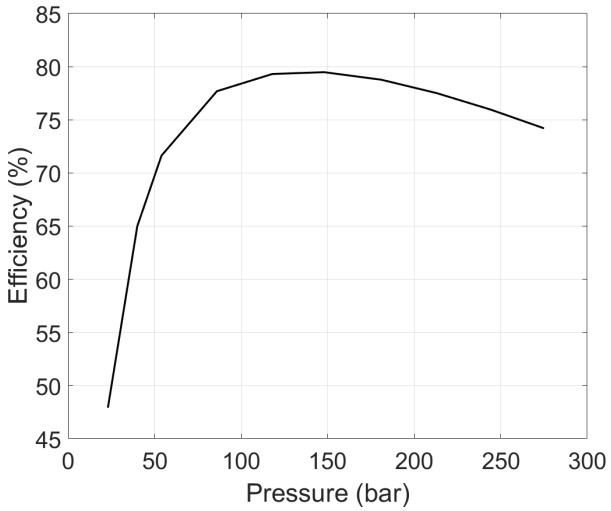

Figure 4. Hydrostatic transmission efficiency (pump displacement = 150 cm^3; pump shaft speed = 2000 rpm).

As for the hydraulic system for the lifting arm and the extension boom, the following approach was adopted: firstly, the hydro-mechanical system was modelled considering an hydraulic pump, two four-way directional valves and two double-acting hydraulic cylinders. Secondly, the lifting arm and extension boom were modelled using Simscape

Multibody. For the development of the Multibody, the kinematics of the system was defined in accordance with [46]. In detail, the Multibody model included two hydraulic cylinders, one to control the lifing angle of the telescopic arm, and the other to control the extension of the boom. The hydraulic pistons were modelled as cylindrical solids and were connected to the cylinder barrels, modelled as revolved solids, by means of prismatic joints. The head of the hydraulic piston for the regulation of the lift angle was connected to the body of the lifting arm by means of a bearing joint. The bottom of the hydraulic cylinders was connected to the chassis of the vehicle using revolute joints. The body, representing the bucket, was linked to the head of the hydraulic boom using a revolute joint that was controlled so that it maintained the same angle with respect to the pavament during lifting operations. To take into account the presence of a mass in the bucket, an external force, as a function of time, was added and placed in the middle of the bucket. After defining the Multibody system, it was interfaced with the hydro-mechanical network so that the translational force coming from the physical network model was used to evaluate the movement of the multibody joints, and, as a consequence, of the lifting arm and extension boom. As a feedback from the multibody network, the hydraulic cylinders received the information of position and speed. The two four-way directional valves were used as actuators for the hydraulic cylinders. A pressure relief valve, with a pressure setting of 300 bar, was introduced in the hydraulic system to prevent excessive peaks in the circuit.

The internal combustion engine was modelled using its speed-torque profile. As for the fuel consumption, the fuel consumption estimation model described in [47] was adopted. According to this model, the brake-specific fuel consumption (BSFC) is evaluated using a polynomial curve that is a function of the engine speed and torque:

$$Z = b_1 + b_2 \cdot X + b_3 \cdot Y + b_4 \cdot X^2 + b_5 \cdot X \cdot Y + b_6 \cdot Y^2 \quad (5)$$

where:

- X is the normalized engine speed: $X = \dfrac{n}{n_{nom}} \cdot 100.$
- Y is the normalized brake torque: $Y = \dfrac{T}{T_{nom}} \cdot 100.$
- Z is the normalized BSFC: $Z = \dfrac{BSFC}{BSFC_{min}} \cdot 100.$
- $b_{i=1,\ldots,6}$ are the polynomial coefficients.

According to this model, the region of the minimum BSFC is usually located at about 73–77% of the nominal engine rotational speed and at a high load, namely 85–95% of the nominal torque. Finally, the power required by the vehicle auxiliaries was considered, assuming that they require around 8% of the rated engine power. The numerical model developed in MATLAB/Simulink is shown in Figure 5.

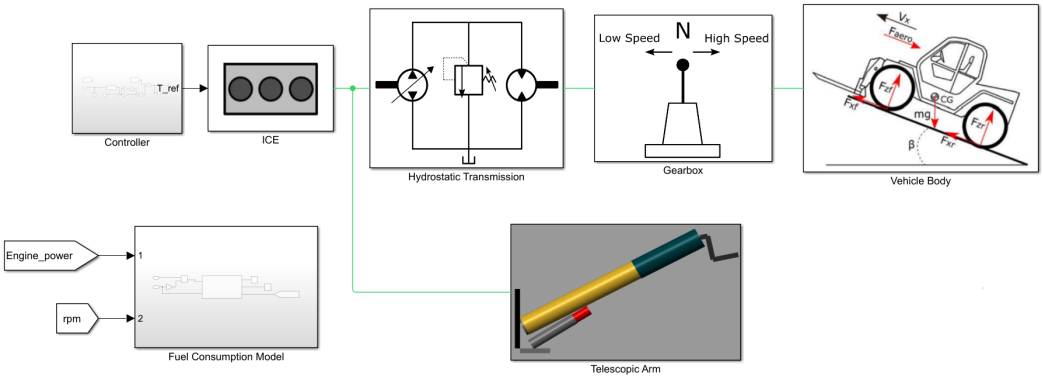

Figure 5. Numerical model for the traditional powertrain.

3.2. Fuel Cell Vehicle Numerical Modelling

As for the fuel cell vehicle, the authors assumed that, apart from the engine, all the other subparts are the same as the traditional counterpart. Thus, the vehicle chassis, transmission, hydraulic system, lifting arm and extension boom were not modified. As for the powertrain, the following elements were considered during the modelling:

- The fuel cell system.
- The battery pack.
- The power converters.
- The electric motor.

The fuel cell system was modelled as an equivalent circuit using the following equation [22,48]:

$$V_{stack} = N_{cell} * (E_{Nernst} - V_{act} - V_{ohm} - V_{conc}) \quad (6)$$

where V_{stack} is the overall voltage of the fuel cell stack, N_{cell} is the number of cells in the stack, E_{Nernst} is the Nernst voltage, V_{act} represents the voltage loss due to activation, V_{ohm} represents the voltage loss due to internal ohmic resistance and V_{conc} stands for the voltage loss due to concentration (mass transport processes). Given the operative conditions, the following equations can be used to determine the voltage of the fuel cell stack:

$$E_{Nernst} = 1.229 + (T - 298) * \frac{-44.43}{2F} + \frac{R_g T}{2F} * ln(\frac{p_{H_2} p_{O_2}^{1/2}}{p_{H_2O}}) \quad (7)$$

$$V_{act} = \frac{R_g T}{2F\alpha} * log(\frac{i_{dens}}{i_0}) \quad (8)$$

$$V_{ohm} = R_{ohm} * i_{dens} \quad (9)$$

$$V_{act} = \frac{R_g T}{2F} * log(1 - \frac{i_{dens}}{i_{lim}}) \quad (10)$$

where:

- T is the stack temperature.
- F is the Faraday constant, equal to 96,485.33 C/mol.
- R_g is the ideal gas constant.
- p_{H_2}, p_{O_2} and p_{H_2O} represent, respectively, the hydrogen, oxygen and water partial pressures.
- α is the charge transfer coefficient.
- i_{dens} is the current density.
- i_0 is the exchange current density.
- R_{ohm} is the ohmic resistance.
- i_{lim} is the maximum current density.

Using the aforementioned equations with operational parameters generally adopted for these systems, the voltage–current curve reported in Figure 6 was obtained. As for the hydrogen consumption, the following equation was used:

$$q_{H_2} = \frac{N_{cell} i_{FC} MM_{H_2}}{2F} \quad (11)$$

where q_{H_2} is the hydrogen mass flow that reacts at the anode, MM_{H_2} is the H_2 molar mass and i_{FC} is the current delivered by the fuel cell stack.

However, the sole fuel cell stack model is not enough to properly simulate the behaviour of the whole fuel cell system. Indeed, to effectively evaluate the system efficiency, the power absorbed by the Balance of Plant (BoP) system should be considered [22,26,33]. According to [49], the fuel cell BoP approximately absorbs around 13–19% of the power delivered by the stack. To address this issue, the power required by the BoP was added into the numerical model as an additional electrical load on the DC bus.

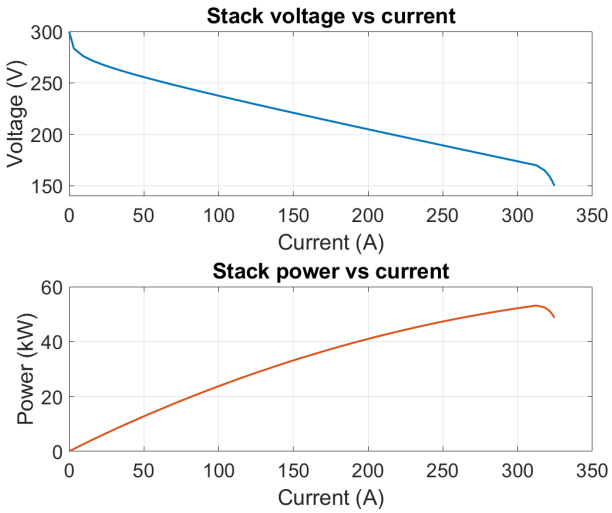

Figure 6. Fuel Cell stack curves.

As for the battery pack, it was modelled using a dynamic equivalent circuit model [50,51]. In detail, the dual polarization model shown in Figure 7 was used. In the adopted model, resistors and capacitors were considered constant, while the open circuit voltage was modelled as a function of the SOC. The SOC was evaluated using a simple Coulomb counting mode, neglecting more detailed models.

Concerning the power converters, their efficiency was considered constant and equal to 95%. Finally, the electric motor was modelled considering the torque-dependent electrical losses and the speed-dependent electrical losses. Moreover, a series resistance was considered between the DC bus and the electric motor, in order to take into account the ohmic losses along the wires. The numerical model of the fuel cell hybrid electric telehandler is shown in Figure 8.

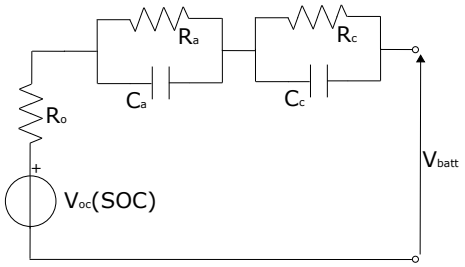

Figure 7. Dynamic equivalent circuit model for the battery pack.

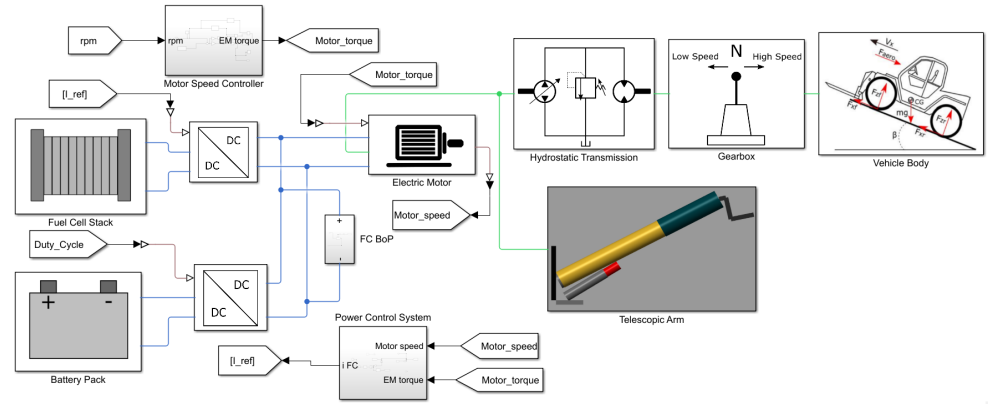

Figure 8. Fuel Cell hybrid electric telehandler numerical model.

4. Numerical Simulations

4.1. Powertrain Control Strategy

Regarding the traditional vehicle, the internal combustion engine is set at a fixed speed of 2000 rpm and is controlled using a proportional-integral (PI) controller. The vehicle speed is determined by changing the displacement of the pump in the hydrostatic transmission. As for the hydraulic system, it is controlled acting on the pump and on the valves. As for the fuel cell hybrid electric vehicle, the approach is the same. However, since there are two power sources, namely the fuel cell stack and the battery pack, an energy management strategy must be defined to determine how to split the power required by the motor between the two different sources. For this preliminary analysis, the authors opted for a simple power follower control strategy. Power follower strategies, like other rule-based strategies, have the advantage of easy implementation and integration in embedded controllers, and are able to provide good and stable control even if they could lead to not optimal fuel economy or component degradation with respect to optimization-based energy management strategies [52]. However, the authors deemed that a simple power follower strategy was sufficient for this preliminary analysis. The main goal of the strategy is to operate in a charge-sustaining mode without exceeding the power limits of the fuel cell. To prevent fast degradation, the fuel cell stack should operate following the low frequency component of the load. Indeed, sudden and intense changes in the fuel cell power output could reduce its lifetime due to reactant starvation or membrane flooding processes [41,53–55]. In fuel cell powertrains, the power conditioning units are represented by the DC-DC converters, which can be controlled both in the voltage or the current reference mode. Therefore, to perform the power split between the fuel cell and the battery pack, the power control system evaluates a reference current for the fuel cell, which is used to control the unidirectional DC-DC converter. In detail, the current reference is evaluated, using a predefined set of rules, according to the current required by the electric motor. To operate in a charge-sustaining mode, the control strategy adopts penalty factors depending on the batteries' State of Charge (SOC). The fuel cell minimum output was set to be equal to its idle power and assumed to be approximately 10% of the nominal stack power. A schematic representation of the control strategy for the fuel cell powertrain is represented in Figure 9. As for the bidirectional DC-DC converter on the batteries' side, it was used to control the voltage of the DC-DC bus, which was set to 640 V.

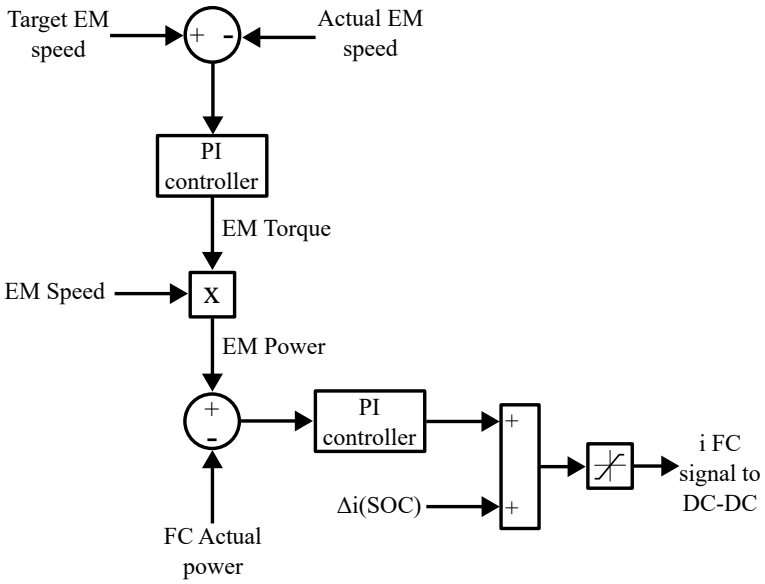

Figure 9. Fuel Cell hybrid electric powertrain control strategy.

4.2. Simulated Work Scenarios

To assess the powertrain performance and to perform a comparison between the traditional vehicle and the fuel cell hybrid electric counterpart, the simulations were defined in order to evaluate the behaviour of the two vehicles in terms of acceleration time, overcoming slopes, fuel economy and environmental impact. Moreover, the simulations were also used to assess the maximum change rate, expressed in kW/s, in the fuel cell power output. For the performance assessment, the following tests were performed:

- Acceleration from 0 to 40 km/h with no load.
- Acceleration from 0 to 40 km/h, handling a trailer with a total weight of 4200 kg.
- Maximum speed at 20% of slope.
- Maximum approachable slope, handling a load of 4200 kg.
- Maximum approachable slope at 15 km/h.

The acceleration tests were conducted using the high-speed regime gear. Thus, during the acceleration, no gearshifting is performed. As for the slope tests, they were conducted with a standing start at the prescribed slope. The friction coefficients for the wheel-ground contact were defined according to a pavement road. To assess the fuel economy, a work cycle based on a typical real operartive scenario was defined. The proposed real work scenario was based on the one defined in [56], which corresponds to the telehandler picking and handling a load, and is composed of the following phases:

- Approaching: the vehicle approaches to the load that must be moved.
- Loading: the vehicle picks up the load using the telescopic arm; in this phase, the telescopic arm lift angle starts to increase, lifting the load and reaching a maximum angle of approximately 50 degrees, and then decreases to 25 degrees, which is the angle at which the vehicle handles the load during the transfer phase.
- Release: the vehicle moves back from the point where the load was located; the telescopic arm maintains a constant lift angle of 25 degrees.
- Transfer with load: the vehicle handles the load up to 15 km/h and reaches the point where the load must be placed; the lifting angle remains constant at 25 degrees during the whole phase.
- Unloading: the vehicle deposits the load by means of the telescopic arm and the extension boom; in this phase, the lift angle increases to 50 degrees, then the extension of the telescopic boom starts to increase, reaching 1000 mmm, and then the load is placed; after that, the extension boom returns to 0 mm and the lift angle decreases to 0 degrees.
- Transfer without load: the vehicle moves back without the load.

The work cycle is reproduced twice with two different loads, one corresponding to approximately 3000 kg and the other to 1500 kg. As for the wheel–ground contact, in a real work scenario the friction coefficients were defined considering off-road conditions.

5. Results and Discussion

5.1. Simulations Results

5.1.1. Performance Tests

The results of the performance evaluation tests are reported in Table 4. As expected, the two powertrains showed approximately the same performances. The traditional vehicle performed slightly better due to the higher power of the internal combustion engine in the range 1400–1900 rpm with respect to the electric motor. As for the slope tests, it should be highlighted that the maximum performance was limited, not by the capacity of the wheel to transmit force to the ground, but by the available power at the driveline downstream from the hydrostatic transmission.

Table 4. Performance test results.

Performed Test	Traditional Vehicle	Fuel Cell Hybrid Vehicle
Time for 0–40 km/h no load	12 s	12.5 s
Time for 0–40 km/h with 4200 kg	20 s	21 s
Max speed with 20% slope	9 km/h	8 km/h
Max slope with 4200 kg	15% @ 5 km/h	15% @ 5 km/h
Max slope at 15 km/h	12%	10%

However, the aim of the performance tests was also to evaluate the behaviour of the fuel cell powertrain under peak power conditions. Therefore, the maximum instantaneous hydrogen consumption, the maximum C-rates in charge and discharge for the battery pack and the mean change rate in the fuel cell power output were evaluated. The results are shown in Table 5. As stated, the acceleration tests were the most impactful in terms of stress on both the FC system and the battery pack.

Table 5. Fuel cell powertrain behaviour during the performance tests.

	FC System		Battery Pack	
	Max Change Rate (kW/s)	Max H_2 Flow (g/s)	Max Charge C-Rate	Max Discharge C-Rate
0–40 km/h no load	8.7	0.69	0.6	6.3
0–40 km/h 4200 kg	5.1	0.66	0.35	6.1
Top speed 20% slope	4.2	0.47	0.35	5.6
Max slope with 4200 kg	3.4	0.52	0.35	5.2
Max slope at 15 km/h	4.0	0.55	0.35	4.9

5.1.2. Real Work Scenario

The simulation results for the real work scenario are reported in Figures 10 and 11. As can be observed from the figure, the 0–15 km/h acceleration phase is the most demanding one due to the high vehicle mass, with a peak power of approximately 55 kW when carrying a 3000 kg load. Also in this case, the simulation was used to evaluate the behaviour of the fuel cell powertrain, and the results are summarized in Table 6.

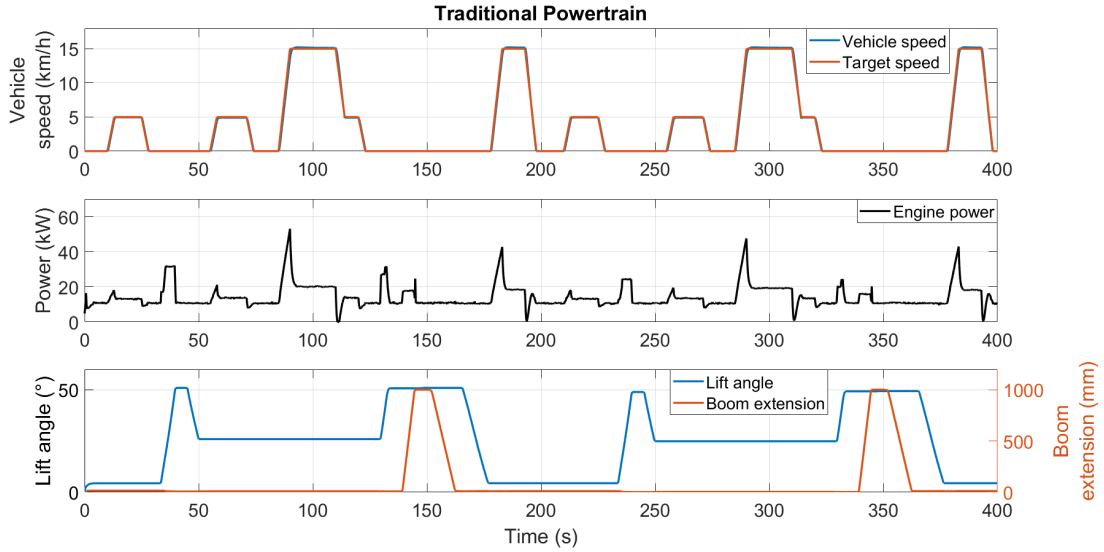

Figure 10. Real work scenario results for the traditional powertrain.

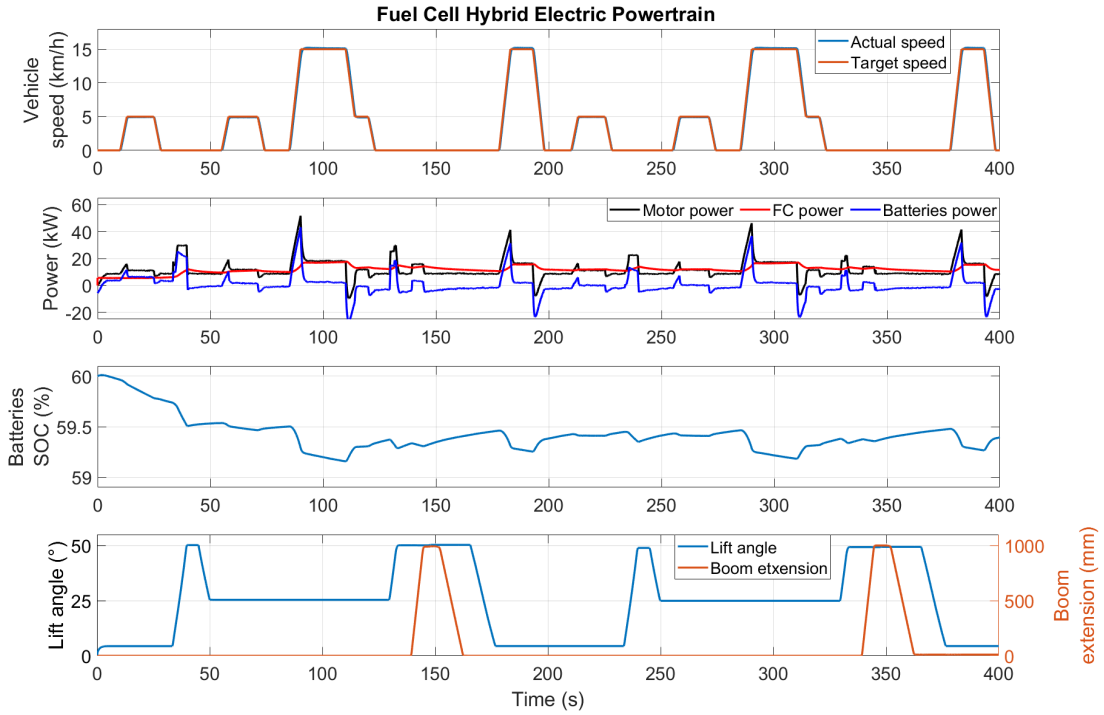

Figure 11. Real work scenario results for the fuel cell hybrid electric powertrain.

Table 6. Fuel cell powertrain behaviour during the real work scenario test.

Parameter	Value
Max FC change rate (kW/s)	4.04
Max H_2 consumption (g/s)	0.23
Max charging C-rate	1.7 C
Max discharging C-rate	2.7 C
Total H_2 consumption (g)	60.4

5.2. Fuel Cell System Degradation Analysis

To estimate the fuel cell system durability, in this section a degradation analysis, based on models available in the literature, is proposed. According to [41], the lifetime of a fuel cell system can be defined as follows:

$$T_{lifetime,FC} = \frac{\Delta P}{k_p(\beta_1 n_1 + \beta_2 n_2 + \beta_3 t_1 + \beta_4 t_2)} \quad (12)$$

where $T_{lifetime,FC}$ is the expected lifetime, ΔP is the maximum acceptable reduction in the fuel cell output performance, generally fixed at 10%; $\beta_{i=1,\ldots,4}$ are the performance degradation rates related, respectively, to load change cycling, start-stop cycling, idle condition and high power condition; n_1, n_2, t_1 and t_2 are the load changing cycles, start and stop cycles, idle condition time and high-power condition time; and finally, k_p is an accelerating coefficient. The main limitations of this model are related to the coefficients that may not be updated since the study was published in 2008. However, this model is considered a key reference for fuel cells' degradation evaluation and was used in more recent studies that proposed this kind of analysis [53,54,57,58]. Nevertheless, fuel cell systems' durability has experienced relevant improvements in the last few years. Indeed, according to [59], in 2007, the state of the art in terms of the durability for fuel cell systems in automotive applications corresponded to 1250 h. Considering the present DOE targets [60], the ultimate targets in terms of durability are set to 8000 h. However, to be conservative, the authors opted for considering the coefficients used in [41]. In [53], an additional coefficient, related to the natural degradation of the fuel cell due to material aging, was

added. However, no details are provided about how that coefficient was determined. Therefore, in the present paper, the authors opted for not considering it. The adopted values for the degradation analysis of the fuel cell systems are reported in Table 7. The degradation analysis was conducted considering the real work scenario, which should be the most common operating condition, and the 0–40 km/h acceleration test with no load, which was the test that exhibited the highest change rate in the fuel cell power output. The results in terms of the expected life, considering a maximum decrease of 10% in the system performance for the two scenarios, are reported in Table 8. As it can be stated, severe and frequent accelerations can lead to a reduction in the lifetime expectancy. On the contrary, the lifetime estimation considering the real work scenario exceeded the DOE ultimate target of 8000 h. However, the authors wanted to highlight that the adopted powertrain control strategy was not optimized through an optimization process, but was a simplified control based on a power follower algorithm with a low dynamic response of the fuel cell system. The aim was to roughly reduce the load changes in the fuel cell power output, but no optimization algorithm was used. Future works might focus on a more developed aging-aware control strategy.

Table 7. Adopted coefficients for the degradation analysis of the fuel cell system. The coefficients were defined according to [41].

Factor	Condition	Value	Unit
β_1	Load cycling	5.93×10^{-5}	%/cycle
β_2	Start and Stop	1.96×10^{-3}	%/cycle
β_3	Idling ($P_{out,FC} \leq 10\%$)	1.26×10^{-3}	%/h
β_4	High power ($P_{out,FC} \geq 90\%$)	1.47×10^{-3}	%/h
k_p	-	1.72	-

Table 8. Degradation analysis results for the two considered scenarios: real work scenario and 0–40 km/h acceleration test with no load.

Test Scenario	FC System Expected Life
0–40 km/h acceleration test no load	1257 h
Real work scenario	9410 h

5.3. Environmental Analysis

To assess the environmental performances of the fuel cell powertrain with respect to the traditional model, the authors opted for using a WtW approach. This approach is useful for evaluating the environmental performances of a vehicle during its use phase, since it accounts for the emissions related to fuel extraction, treatment, distribution and conversion [61]. The authors opted for considering the use of hydrogen from the actual hydrogen production mix, which is mainly from fossil fuel resources; hydrogen from steam methane reforming but with a carbon capture system, namely blue hydrogen; and hydrogen from electrolysis, based on the grid, nuclear and renewables. The authors also decided to consider the global warming potential as an impact category, since the climate change issue is one of the major challenges that humankind has to face within the near future, and the efforts to mitigate it are among the main reasons behind the electrification of powertrains. For hydrogen from the actual production mix and Diesel consumption, the WtW factors for the equivalent CO_2 emissions were derived from [8], while the coefficients for the other considered hydrogen production methods were taken from [34]. The WtW emission factors adopted for the environmental impact analysis are summarized in Table 9. The factor for the hydrogen from electrolysis based on renewables was determined considering the average values for electrolysis based on biomass, wind and solar. As for the electrolysis based on the grid, the WtW emission factor may vary depending on the country, since it mainly depends on the electricity production mix. The analysis was conducted considering the real work scenario. The results are shown

in Table 10. As can be stated, with the present hydrogen production mix, the fuel cell powertrain can reduce the CO_2 equivalent emissions of 68.6%. However, with cleaner and greener production methods, the emission reduction can be enhanced. In detail, the emission reduction can reach 97.5% using electrolysis with electricity from nuclear, and 92.6% using hydrogen from electrolysis powered with electricity from renewables. Furthermore, a noticeable reduction in GHG emissions can also be achieved using hydrogen produced from fossil fuel resources with carbon capture technologies. Instead, with the production of hydrogen from electrolysis using the electricity grid mix, no effective emission reduction might be obtained. This demonstrates that coupling electrolysis with clean electricity is a key element to achieve greater results in terms of the environmental impact reduction in hydrogen-powered vehicles. The results obtained from the environmental analysis were coherent with other studies that estimated the life cycle CO_2 emissions of fuel cell vehicles to be less than 50% of that of the traditional counterpart, with very low-use phase impacts when hydrogen is produced from renewables [62–64].

Table 9. WtW equivalent emission factors for Diesel and H_2 according to [8,34].

Emission Source	WtW Emission Factor	Unit
Diesel	3.18	kg CO_2-eq./L
Actual Hydrogen production mix	9.13	kg CO_2-eq./kg
Blue Hydrogen	3.70	kg CO_2-eq./kg
Hydrogen from Electrolysis (based on nuclear)	0.71	kg CO_2-eq./kg
Hydrogen from Electrolysis (based on grid)	29.21	kg CO_2-eq./kg
Hydrogen from Electrolysis (based on renewables)	1.87	kg CO_2-eq./kg

Table 10. Environmental impact comparison for the real work scenario.

	Fuel Consumptions	
Diesel consumption	0.55 L	
Hydrogen consumption	60.4 g	
Fuel	**Emissions (kg CO_2-eq.)**	**Difference (%)**
Diesel	1.75	-
Hydrogen (actual production mix)	0.55	−68.6
Blue Hydrogen	0.22	−87.4
Hydrogen from Electrolysis (based on nuclear)	0.043	−97.5
Hydrogen from Electrolysis (based on grid)	1.76	+0.1
Hydrogen from Electrolysis (based on renewables)	0.13	−92.6

5.4. Discussion

The degradation and environmental analysis showed that fuel cell powertrains can be a feasible solution to mitigate the impact of Non-Road Mobile Machinery on the environment in terms of equivalent CO_2 emissions. However, the applicability of these systems on a real vehicle is not straightforward. From a technical point of view, one of the major challenges is the integration of the fuel cell system on-board the vehicle. Another technical issue is regarding the on-board hydrogen storage system. Considering the simulation results for the real work scenario, to operate for 8 h straight without the need for refuelling, the hydrogen storage system should be able to stock around 4.5 kg of H_2. This storage capacity requirement can be satisfied implementing a modern type IV tank, which can store 5.8 kg of hydrogen in its gaseous form at 700 bar. The system weighs approximately 133.6 kg and has a volume of 229.6 litres [65]. Alternatively, to reduce the volume of the storage system, another possible solution is represented by metal hydride tanks. These systems can reach higher volumetric densities, up to five times higher, but have a lower gravimetric density compared to gaseous tanks [66]. Furthermore, metal hydride tanks require a heat management system to operate properly, thus a higher complexity of the whole powertrain

might be introduced [67]. On the contrary, the adoption of a type IV storage tank involves safety issues that must be considered during the design stage of the vehicle [68]. However, the most insidious challenges are related to other factors that go beyond the technical issues related to the realization of a first propotype. As stated in [38], one of the most critical factors that is slowing the diffusion of fuel cell systems on vehicular applications is the early stage of development of the hydrogen refuelling network. Furthemore, the hydrogen refueling infrastructure requires an investment cost that is extremely high compared to the cost of other fuel refueling stations [69]. Another important challenge is represented by the higher purchasing cost of fuel cell vehicles with respect to their traditional and battery electric counterpart [70]. Indeed, the hydrogen tanks and the stack are the most expensive components of the fuel cell system due to the presence of expensive materials, such as platinum, used as catalyst in the stack; and carbon fibre, used to manufacture the type IV tank [39,65,71]. To reduce the cost of the fuel cell systems, DOE targets have been defined for the future [72,73]. Along with the problem related to the high cost, another aspect that must be faced is the lack of consumer awareness about fuel cell vehicles, which results in a distorted perception about their safety and performances [74]. According to [75], in vehicle users there is a combination of aversion to high purchase costs and negative perceptions of environmental benefits from adopting hydrogen that is creating a barrier between the market and fuel cell vehicles. As a consequence, overcoming the problem of a social attitude towards the acceptance of fuel cell vehicles is mandatory to promote their diffusion [76]. However, environmental policies and regulations might be important drivers for the adoption of hydrogen technologies [77,78]. In this context, the European Community is pursuing the goal of reaching a reduction of 55% in net greenhouse gas emissions for 2030 with respect to the emission levels of 1990, and of achieving carbon neutrality for 2050 [79]. However, the sector of Non-Road Mobile Machinery is at an earlier stage of decarbonisation with respect to passenger vehicles. Indeed, the actual regulation for Non-Road Mobile Machinery focuses on the emission levels of CO, HC, NO_x and particulate matter, while no limits for CO_2 are, at present, introduced [80]. Nevertheless, the limits for the aforementioned pollutants are becoming more and more stringent and are requiring more complex and bulky exhaust gas aftertreament systems. Thus, this poses technical challenges that may be drivers for the adoption of fuel cell systems, which instead do not require an aftertreatment system since they produce water at the exhaust.

6. Conclusions

Fuel cell hybrid electric powertrains represent a promising strategy to replace traditional internal combustion engines in the sector of Non-Road Mobile Machinery. Indeed, fuel cell vehicles feature zero local emission levels, high-energy density and low refuelling time, which make them more interesting than battery electric vehicles for applications where endurance and productivity are crucial with a view to be competitive on the market. In this article, the preliminary design of a fuel cell hybrid electric powertrain for a telehandler was presented. The proposed system is characterized by the presence of a PEMFC stack, with a rated power approximately equal to 50% of the electric motor nominal power, whose role is to satisfy the low-frequency component of the external load, and a battery pack, which has to handle the high frequency part of the load to avoid the fast degradation of the fuel cell system. To make a comparison between the proposed system and the traditional one, numerical models of both the powertrain were built in a MATLAB/Simulink environment. The modelling included a Multibody model to simulate the use of the telescopic arm and the extension boom. For the simulations, the authors developed a simple charge-sustaining power follower strategy to determine the power split between the fuel cell and the battery pack. The simulations were regarding two type of tests: peak power performance tests and the real work scenario simulation test. The first set of tests aimed at evaluating both the performances in terms of the acceleration and overcoming of slopes, and the behaviour of the fuel cell powertrain in terms of stress on its main components. On the contrary, the real work scenario test aimed at evaluating the

fuel economy and the environmental impact of the powertrains during a typical operative scenario, characterized by the handling of loads by the mean of the telescopic arm. The results of the simulations are summarized as follows:

- The fuel cell powertrain was able to show almost the same performances of the traditional one without excessive stress on its components; indeed, a degradation analysis was conducted to address the fuel cell durability issue.
- The most stressful tests for the fuel cell powertrain were the acceleration tests, since the max change rate in the fuel cell output was equal to 15% of the rated stack power per second, and the max discharge C-rate of the battery pack was equal to 6.3.
- During the real work scenario test, the fuel cell powertrain showed a reduction in terms of the equivalent CO_2 emissions of 69% with respect to the traditional powertrain; this result was obtained considering the use of grey hydrogen for the fuel cell system and can be improved using hydrogen from a cleaner production mix.

Therefore, the authors concluded that the adoption of fuel cell systems are a feasible solution for replacing traditional internal combustion engines in telehandlers, since they can have the same performances without excessive degradation and with a reduction in terms of equivalent CO_2 emissions. However, a higher purchase cost is expected for the fuel cell vehicle with respect to the diesel-powered counterpart. Therefore, to be competitive on the market, consumers' awareness of environmental performances and safety of the proposed powertrain is mandatory. A further analysis might be regarding the development of a more detailed and optimized energy management strategy, with the aim of minimizing fuel consumption, component degradation or both of them according to a predefined objective function. As demonstrated in the literature, the adoption of optimization algorithms can enhance the powertrain performance. Other future works could investigate the possibility of introducing supercapacitors to reduce batteries' degradation. Furthermore, due to the lack of experimental data, the adoption of a monitoring device that could be installed on-board a real telehandler, to outline its realistic mission profile, could be the subject of research and attention. To immprove the simulation reliability, tests on a scaled test bench with a real fuel cell system might be conducted in the future. To promote circular economy, another subject of research could be the integration of green hydrogen production systems, powered using electricity from renewable sources, to locally produce clean hydrogen to be used in the vehicle. A typical case study might be a farm with an electrolyser powered using renewable sources. In that scenario, the farm is able to produce green hydrogen with very low equivalent CO_2 emissions using water and, for example, electricity coming from solar panels. That hydrogen can be used to power the vehicle. Furthermore, the water produced at the exhaust can be re-used in the electrolyser for the hydrogen production.

Author Contributions: Conceptualization, V.M., F.M. and A.S.; methodology, V.M., F.M. and A.S.; software, V.M., F.M. and A.S.; validation, V.M., F.M. and A.S.; formal analysis, V.M., F.M. and A.S.; investigation, V.M., F.M. and A.S.; data curation, V.M., F.M. and A.S.; writing—original draft preparation, V.M., F.M. and A.S.; writing—review and editing, V.M., F.M. and A.S.; visualization, V.M., F.M. and A.S.; supervision, V.M., F.M. and A.S. All authors have read and agreed to the published version of the manuscript.

Funding: This research received no external funding.

Institutional Review Board Statement: Not applicable.

Informed Consent Statement: Not applicable.

Data Availability Statement: Data are contained within the article.

Conflicts of Interest: The authors declare no conflicts of interest.

References

1. Anenberg, S.C.; Achakulwisut, P.; Brauer, M.; Moran, D.; Apte, J.S.; Henze, D.K. Particulate matter-attributable mortality and relationships with carbon dioxide in 250 urban areas worldwide. *Sci. Rep.* **2019**, *9*, 11552. [CrossRef]
2. McDuffle, E.E.; Martin, R.V.; Spadaro, J.V.; Burnett, R.; Smith, S.J.; O'Rourke, P.; Hammer, M.S.; van Donkelaar, A.; Bindle, L.; Shah, V.; et al. Source sector and fuel contributions to ambient PM2.5 and attributable mortality across multiple spatial scales. *Nat. Commun.* **2021**, *12*, 3594. [CrossRef]
3. Zhu, L.; Ge, X.; Chen, Y.; Zeng, X.; Pan, W.; Zhang, X.; Ben, S.; Yua, Q.; Xin, J.; Shao, W.; et al. Short-term effects of ambient air pollution and childhood lower respiratory diseases. *Sci. Rep.* **2017**, *7*, 4414. [CrossRef] [PubMed]
4. Eom, J.; Hyun, M.; Lee, J.; Lee, H. Increase in household energy consumption due to ambient air pollution. *Nat. Energy* **2020**, *5*, 976–984. [CrossRef]
5. Dai, C.; Qin, X.S.; Zhang, X.L.; Liu, B.J. Study of climate change impact on hydro-climatic extremes in the Hanjiang River basin, China, using CORDEX-EAS data. *Weather Clim. Extremes* **2022**, *38*, 100509. [CrossRef]
6. Taghizadeh-Hesary, F.; Taghizadeh-Hesary, F. The Impacts of Air Pollution on Health and Economy in Southeast Asia. *Energies* **2020**, *13*, 1812. [CrossRef]
7. McCarthy, P.; Rasul, M.G.; Moazzem, S. Analysis and comparison of performance and emissions of an internal combustion engine fuelled with petroleum diesel and different bio-diesels. *Fuel* **2011**, *90*, 2147–2157. [CrossRef]
8. Buberger, J.; Kersten, A.; Kuder, M.; Eckerle, R.; Weyh, T.; Thiringer, T. Total CO_2-equivalent life-cycle emissions from commercially available passenger cars. *Renew. Sustain. Energy Rev.* **2022**, *159*, 112158. [CrossRef]
9. Onat, N.C.; Kucukvar, M.; Tatari, O. Towards Life Cycle Sustainability Assessment of Alternative Passenger Vehicles. *Sustainability* **2014**, *6*, 9305–9342. [CrossRef]
10. European Parliament. Available online: https://www.europarl.europa.eu/news/en/headlines/economy/20221019STO44572/eu-ban-on-sale-of-new-petrol-and-diesel-cars-from-2035-explained (accessed on 3 January 2024).
11. Rietmann, N.; Hugler, B.; Lieven, T. Forecasting the trajectory of electric vehicle sales and the consequences for worldwide CO_2 emissions. *J. Clean. Prod.* **2020**, *261*, 121038. [CrossRef]
12. Martelli, S.; Mocera, F.; Somà, A. Carbon Footprint of an Orchard Tractor through a Life-Cycle Assessment Approach. *Agriculture* **2023**, *13*, 1210. [CrossRef]
13. Martelli, S.; Mocera, F.; Somà, A. New Challenges Towards Electrification Sustainability: Environmental Impact Assessment Comparison between ICE and Hybrid-Electric Orchard Tractor. In Proceedings of the 2023 JSAE/SAE Powertrains, Energy and Lubricants International Meeting, Kyoto, Japan, 29 August–1 September 2023. [CrossRef]
14. Cunanan, C.; Tran, M.-K.; Lee, Y.; Kwok, S.; Leung, V.; Fowler, M. A Review of Heavy-Duty Vehicle Powertrain Technologies: Diesel Engine Vehicles, Battery Electric Vehicles, and Hydrogen Fuel Cell Electric Vehicles. *Clean Technol.* **2021**, *3*, 474–489. [CrossRef]
15. Mocera, F.; Martini, V. Numerical Performance Investigation of a Hybrid eCVT Specialized Agricultural Tractor. *Appl. Sci.* **2022**, *12*, 2438. [CrossRef]
16. Mocera, F.; Martini, V.; Somà, A. Comparative Analysis of Hybrid Electric Architectures for Specialized Agricultural Tractors. *Energies* **2022**, *15*, 1944. [CrossRef]
17. Mocera, F.; Martelli, S.; Costamagna, M. Dynamic behaviour of a battery pack for agricultural applications. *Conf. Ser. Mater. Sci. Eng.* **2022**, *1214*, 012032. [CrossRef]
18. Mocera, F.; Somà, A. Analysis of a Parallel Hybrid Electric Tractor for Agricultural Applications. *Energies* **2020**, *13*, 3055. [CrossRef]
19. Dalboni, M.; Santarelli, P.; Patroncini, P.; Soldati, A.; Concari, C.; Lusignani, D. Electrification of a Compact Agricultural Tractor: A Successful Case Study. In Proceedings of the 2019 IEEE Transportation Electrification Conference and Expo (ITEC), Novi, MI, USA, 19–21 June 2019; IEEE: Piscataway, NJ, USA, 2019; pp. 1–6. [CrossRef]
20. Available online: https://www.farm-equipment.com/articles/19849-antonio-carraro-srx-hybrid-tractor (accessed on 15 February 2024).
21. Available online: https://www.landini.it/as/landini-rex4-full-hybrid-technical-innovation-at-eima-2022/ (accessed on 15 February 2024).
22. Martini, V.; Mocera, F.; Somà, A. Numerical Investigation of a Fuel Cell-Powered Agricultural Tractor. *Energies* **2022**, *15*, 8818. [CrossRef]
23. Di Ilio, G.; Di Giorgio, P.; Tribioli, L.; Bella, G.; Jannelli, E. Preliminary design of a fuel cell/battery hybrid powertrain for a heavy-duty yard truck for port logistics. *Energy Convers. Manag.* **2021**, *243*, 114423. [CrossRef]
24. Liukkonen, M.; Lajunen, A.; Suomela, J. Feasibility study of fuel cell-hybrid powertrains in non-road mobile machineries. *Autom. Constr.* **2013**, *35*, 296–305. [CrossRef]
25. Mocera, F.; Somà, A.; Martelli, S.; Martini, V. Trends and Future Perspective of Electrification in Agricultural Tractor-Implement Applications. *Energies* **2023**, *16*, 6601. [CrossRef]
26. Martini, V.; Mocera, F.; Somà, A. Design and Experimental Validation of a Scaled Test Bench for the Emulation of a Hybrid Fuel Cell Powertrain for Agricultural Tractors. *Appl. Sci.* **2023**, *13*, 8582. [CrossRef]
27. Ahluwalia, R.K.; Wang, X.; Star, A.G.; Papadias, D.D. Performance and cost of fuel cells for off-road heavy-duty vehicles. *Int. J. Hydrogen Energy* **2022**, *47*, 10990–11006. [CrossRef]
28. De Lorenzo, G.; Ruffo, R.M.; Fragiacomo, P. Preliminary Design of the Fuel Cells Based Energy Systems for a Cruise Ship. *World Electr. Veh. J.* **2023**, *14*, 263. [CrossRef]

29. Waseem, M.; Amir, M.; Lakshmi, G.S.; Harivardhagini, S.; Ahmad, M. Fuel cell-based hybrid electric vehicles: An integrated review of current status, key challenges, recommended policies, and future prospects. *Green Energy Intell. Transp.* **2023**, *2*, 100121. [CrossRef]
30. Louvros, P.; Trivyza, N.L.; Komianos, A.; Boulougouris, E. Fuel cell, ammomnia powered container ship: A case study. *Transp. Res. Procedia* **2023**, *72*, 2245–2252. [CrossRef]
31. Laimon, M.; Yusaf, T. Towards energy freedom: Exploring sustainable solutions for energy independence and self-sufficiency using integrated renewable energy-driven hydrogen system. *Renew. Energ.* **2024**, *222*, 119948. [CrossRef]
32. Tellez-Cruz, M.M.; Escorihuela, J.; Solorza-Feria, O.; Compañ, V. Proton Exchange Membrane Fuel Cells (PEMFCs): Advances and Challenges. *Polymers* **2021**, *13*, 3064. [CrossRef]
33. Lohse-Busch, H.; Stutenberg, K.; Duoba, M.; Liu, X.; Elgowainy, A.; Wang, M.; Wallner, T.; Richard, B.; Christenson, M. Automotive fuel cell stack and system efficiency and fuel consumption based on vehicle testing on a chassis dynamometer at min 18 °C to positive 35 °C temperatures. *Int. J. Hydrogen Energy* **2020**, *45*, 861–872. [CrossRef]
34. Ji, M.; Wang, J. Review and comparison of various hydrogen production methods based on costs and life cycle impact assessment indicators. *Int. J. Hydrogen Energy* **2021**, *46*, 38612–38635. [CrossRef]
35. Das, A.; Peu, S.D. A Comprehensive Review on Recent Advancements in Thermochemical Processes for Clean Hydrogen Production to Decarbonize the Energy Sector. *Sustainability* **2022**, *14*, 11206. [CrossRef]
36. Xu, X.; Zhou, Q.; Yu, D. The future of hydrogen energy: Bio-hydrogen production technology. *Int. J. Hydrogen Energy* **2022**, *47*, 33677–33698. [CrossRef]
37. IEA. Global Hydrogen Review. 2022. Paris. Available online: https://www.iea.org/reports/global-hydrogen-review-2022 (accessed on 4 January 2024).
38. Olabi, A.G.; Abdelkareem, M.A.; Wilberforce, T.; Alami, A.H.; Alkhalidi, A.; Hassan, M.M.; Sayed, E.T. Strength, weakness, opportunities, and threats (SWOT) analysis of fuel cells in electric vehicles. *Int. J. Hydrogen Energy* **2023**, *48*, 23185–23211. [CrossRef]
39. Cano, Z.P.; Banham, D.; Ye, S.; Hintennach, A.; Lu, J.; Fowler, M.; Chen, Z. Batteries and fuel cells for emerging electric vehicle markets. *Nat. Energy* **2018**, *3*, 279–289. [CrossRef]
40. Das, H.S.; Tan, C.W.; Yatim, A.H.M. Fuel cell hybrid electric vehicles: A review on power conditioning units and topologies. *Renew. Sustain. Energy Rev.* **2017**, *76*, 268–291. [CrossRef]
41. Pei, P.; Chang, Q.; Tang, T. A quick evaluating method for automotive fuel cell lifetime. *Int. J. Hydrogen Energy* **2008**, *33*, 3829–3836. [CrossRef]
42. Zhao, X.; Wang, L.; Zhou, Y.; Pan, B.; Wang, R.; Wang, L.; Yan, X. Energy management strategies for fuel cell hybrid electric vehicles: Classification, comparison, and outlook. *Energy Convers. Manag.* **2022**, *270*, 116179. [CrossRef]
43. Available online: https://www.merlo.com/gbr/en/p/telehandlers/medium-capacity-telehandlers/turbofarmer-42-7/ (accessed on 4 January 2024).
44. Somà, A.; Bruzzese, F.; Mocera, F.; Viglietti, E. Hybridization Factor and Performance of Hybrid Electric Telehandler Vehicle. *IEEE Trans. Ind. Appl.* **2016**, *52*, 5130–5138. [CrossRef]
45. Mathworks. *Getting Started with Simscape*; MathWorks: Natick, MA, USA, 2018.
46. Činkelj, J.; Kamnik, R.; Čepon, P.; Mihelj, M.; Munih, M. Closed-loop control of hydrualic telescopic handler. *Autum. Constr.* **2010**, *19*, 954–963. [CrossRef]
47. Golverk, A.A. The Method for Development of a Diesel Engine Universal Performance Map. *SAE Int. J. Fuels Lubr.* **1994**, *103*, 1041–1048.
48. Wang, Y.; Sun, Z.; Chen, Z. Energy management strategy for battery/supercapacitor/fuel cell hybrid source vehicles based on finite state machine. *Appl. Energy* **2019**, *254*, 113707. [CrossRef]
49. Zhang, B.; Wang, X.; Gong, D.; Xu, S. Experimental analysis of the performance of the air supply system in a 120 kW polymer electrolyte membrane fuel cell system. *Int. J. Hydrogen Energy* **2022**, *47*, 21417–21434. [CrossRef]
50. Vergori, E.; Mocera, F.; Somà, A. Battery Modelling and Simulation Using a Programmable Testing Equipment. *Computers* **2018**, *7*, 20. [CrossRef]
51. Lai, X.; Zheng, Y.; Sun, T. A comparative study of different equivalent circuit models for estimating state-of-charge of lithium-ion batteries. *Electrochim. Acta* **2018**, *259*, 566–577. [CrossRef]
52. Yu, P.; Li, M.; Wang, Y.; Chen, Z. Fuel Cell Hybrid Electric Vehicles: A Review of Topologies and Energy Management Strategies. *World Electr. Veh. J.* **2022**, *13*, 172. [CrossRef]
53. Iqbal, M.; Laurent, J.; Benmouna, A.; Becherif, M.; Ramadan, H.S.; Claude, F. Ageing-aware load following control for composite-cost optimal energy management of fuel cell hybrid electric vehicle. *Energy* **2022**, *254*, 124233. [CrossRef]
54. Xu, L.; Mueller, C.D.; Li, J.; Ouyang, M.; Hu, Z. Multi-objective component sizing based on optimal energy management strategy of fuel cell electric vehicles. *Appl. Energy* **2015**, *157*, 664–674. [CrossRef]
55. Chen, H.; Zhao, X.; Zhang, T.; Pei, P. The reactant starvation of the proton exchange membrane fuel cells for vehicular applications: A review. *Energy Convers. Manag.* **2019**, *182*, 282–298. [CrossRef]
56. Mocera, F.; Vergori, E.; Somà, A. Battery Performance Analysis for Working Vehicle Applications. *IEEE Trans. Ind. Appl.* **2020**, *56*, 644–653. [CrossRef]

57. Yang, H.; Sun, Y.; Xia, C.; Zhang, H. Research on Energy Management Strategy of Fuel Cell Electric Tractor Based on Multi-Algorithm Fusion and Optimization. *Energies* **2022**, *15*, 6389. [CrossRef]
58. Jia, C.; Zhou, J.; He, H.; Li, J.; Wei, Z.; Li, K.; Shi, M. A novel energy management strategy for hybrid electric bus with fuel cell health and battery thermal- and health-constrained awareness. *Energy* **2023**, *271*, 127105. [CrossRef]
59. Garland, N.; Benjamin, T.; Kopasz, J. DOE Fuel Cell Program: Durability Technical Targets and Testing Protocols. *ECS Trans.* **2007**, *11*, 923. [CrossRef]
60. Available online: https://www.energy.gov/eere/fuelcells/doe-technical-targets-fuel-cell-systems-and-stacks-transportation-applications (accessed on 12 February 2024).
61. Nordelöf, A.; Messagie, M.; Tillman, A.M.; Ljunggren Söderman, M.; van Mierlo, J. Environmental impacts of hybrid, plug-in hybrid, and battery electric vehicles—what can we learn from life cycle assessment? *Int. J. Life Cycle Asses.* **2014**, *19*, 1866–1890. [CrossRef]
62. Sinha, P.; Brophy, B. Life cycle assessment of renewable hydrogen for fuel cell passenger vehicles in California. *Sustain. Energy Technol. Assess.* **2021**, *45*, 101188. [CrossRef]
63. Teimouri, A.; Kabeh, K.Z.; Changizian, S.; Ahmadi, P.; Mortazavi, M. Comparative lifecycle assessment of hydrogen fuel cell, electric, CNG, and gasoline-powered vehicles under real driving conditions assessment. *Int. J. Hydrogen Energy* **2022**, *47*, 37990–38002. [CrossRef]
64. Teng, Z.; Tan, C.; Liu, P.; Han, M. Analysis on carbon emission reduction intensity of fuel cell vehicles from a life-cycle perspective. *Front. Energy* **2023** . [CrossRef]
65. Hua, T.Q.; Roh,H.-S.; Ahluwalia, R.K. Performance assessment of 700-bar compressed hydrogen storage for light duty fuel cell vehicles. *Int. J. Hydrogen Energy* **2017**, *42*, 25121–25129. [CrossRef]
66. Li, Y.; Teliz, E.; Zinola, F.; Díaz, V. Design of a AB5-metal hydride cylindrical tank for hydrogen storage. *Int. J. Hydrogen Energy* **2021**, *46*, 33889–33898. [CrossRef]
67. Nguyen, H.Q.; Shabani, B. Review of metal hydride hydrogen storage thermal management for use in the fuel cell systems. *Int. J. Hydrogen Energy* **2021**, *46*, 31699–31726. [CrossRef]
68. Guo, L.; Su, J.; Wang, Z.; Shi, J.; Guan, X.; Cao, W.; Ou, Z. Hydrogen safety: An obstacle that must be overcome on the road towards future hydrogen economy. *Int. J. Hydrogen Energy* **2024**, *51*, 105–1078. [CrossRef]
69. Isaac, N.; Saha, A.K. A Review of the Optimization Strategies and Methods Used to Locate Hydrogen Fuel Refueling Stations. *Energies* **2023**, *16*, 2171. [CrossRef]
70. Moon, S.; Lee, Y.-J.; Lee, D.-J. A cost-effectiveness analysis of fuel cell electric vehicles considering infrastructure costs and greenhouse gas emissions: An empirical case study in Korea. *Sustain. Energy Technol. Assess.* **2022**, *54*, 102777. [CrossRef]
71. Usai, L.; Hung, C.R.; Vasquez, F.; Windsheimer, M.; Burheim, O.S.; Strømman, A.H. Life cycle assessment of fuel cell systems for light duty vehicles, current state-of-the-art and future impacts. *J. Clean. Prod.* **2021**, *280*, 125086. [CrossRef]
72. James, B.D. Fuel Cell Cost and Performance Analysis. Available online: https://www.hydrogen.energy.gov/docs/hydrogenprogramlibraries/pdfs/review22/fc353_james_2022_o-pdf.pdf?Status=Master (accessed on 13 February 2024).
73. Houchins, C.; James, B.D. Hydrogen Storage Cost Analysis. Available online: https://www.hydrogen.energy.gov/docs/hydrogenprogramlibraries/pdfs/review22/st235_houchins_2022_p-pdf.pdf?Status=Master (accessed on 13 February 2024).
74. Rawat, A.; Garg, C.P.; Sinha, P. Analysis of the key hydrogen fuel vehicles adoption barriers to reduce carbon emissions under net zero target in emerging market. *Energy Policy* **2024**, *184*, 113847. [CrossRef]
75. Trencher, G.; Wesseling, J. Roadblocks to fuel-cell electric vehicle diffusion: Evidence from Germany, Japan and California. *Transp. Res. D Transp. Environ.* **2022**, *112*, 103458. [CrossRef]
76. Al-Amin, A.Q.; Ambrose, A.F.; Masud, M.M.; Azam, M.N. People purchase intention towards hydrogen fuel cell vehicles: An experiential enquiry in Malaysia. *Int. J. Hydrogen Energy* **2016**, *41*, 2117–2127. [CrossRef]
77. Vallejos-Romero, A.; Cordoves-Sánchez, M.; Cisternas, C.; Sáez-Ardura, F.; Rodríguez, I.; Aledo, A.; Boso, Á.; Prades, J.; Álvarez, B. Green Hydrogen and Social Sciences: Issues, Problems, and Future Challenges. *Sustainability* **2023**, *15*, 303. [CrossRef]
78. Quarton, C.J.; Samsatli, S. How to incentivise hydrogen energy technologies for net zero: Whole-system value chain optimisation of policy scenarios. *Sustain. Prod. Consum.* **2021**, *27*, 1215–1238. [CrossRef]
79. Available online: https://eur-lex.europa.eu/legal-content/EN/TXT/?uri=CELEX:32021R1119 (accessed on 14 February 2024).
80. Available online: https://eur-lex.europa.eu/legal-content/EN/TXT/?uri=CELEX:32016R1628 (accessed on 14 February 2024).